Journal of Power Sources 193 (2009) 376–385

Contents lists available at ScienceDirect

Journal of Power Sources

journal homepage: www.elsevier.com/locate/jpowsour

Energy management of fuel cell/battery/supercapacitor hybrid power source for vehicle applications

Phatiphat Thounthong [a,*], Stephane Raël [b], Bernard Davat [b]

[a] Department of Teacher Training in Electrical Engineering, King Mongkut's University of Technology North Bangkok, 1518, Piboolsongkram Road, Bangsue, Bangkok 10800, Thailand

[b] Groupe de Recherche en Electrotechnique et Electronique de Nancy (GREEN: UMR 7037), CNRS, Nancy Université, INPL-ENSEM 2, avenue de la Forêt de Haye, Vandœuvre-lés-Nancy, Lorraine 54516, France

ARTICLE INFO

Article history:
Received 9 October 2008
Received in revised form
18 November 2008
Accepted 23 December 2008
Available online 8 January 2009

Keywords:
Battery
Converters
Current control
Electric vehicles
Fuel cells
Supercapacitor

ABSTRACT

This paper proposes a perfect energy source supplied by a polymer electrolyte membrane fuel cell (PEMFC) as a main power source and storage devices: battery and supercapacitor, for modern distributed generation system, particularly for future fuel cell vehicle applications. The energy in hybrid system is balanced by the dc bus voltage regulation. A supercapacitor module, as a high dynamic and high power density device, functions for supplying energy to regulate a dc bus voltage. A battery module, as a high energy density device, operates for supplying energy to a supercapacitor bank to keep it charged. A FC, as a slowest dynamic source in this system, functions to supply energy to a battery bank in order to keep it charged. Therefore, there are three voltage control loops: dc bus voltage regulated by a supercapacitor bank, supercapacitor voltage regulated by a battery bank, and battery voltage regulated by a FC. To authenticate the proposed control algorithm, a hardware system in our laboratory is realized by analog circuits and numerical calculation by dSPACE. Experimental results with small-scale devices (a PEMFC: 500-W, 50-A; a battery bank: 68-Ah, 24-V; and a supercapacitor bank: 292-F, 30-V, 500-A) corroborate the excellent control principle during motor drive cycle.

1. Introduction

High prices for gasoline and oil are here to stay. As China, India and other nations rapidly increase their demand for fossil fuels, future fighting over energy looms large. In the meantime, power plants that burn coal, oil and natural gas, as well as vehicles everywhere, continue to pour millions of tons of pollutants and greenhouse gases into the atmosphere annually, threatening the planet.

Well-meaning scientists, engineers, economists and politicians have proposed various steps that could slightly reduce fossil-fuel use and emissions. These steps are not enough. Therefore, this convinces us to dramatically change to hydrogen power, which would be the reasonable answer to this energy crisis problem.

Furthermore, beyond finding new alternative fuels for internal combustion engines (ICEs), researchers are working on hydrogen fuel cells that offer another path toward environmentally acceptable power [1–4]. To produce electricity, most PEM fuel cells must be supplied either with hydrogen or with hydrocarbon compounds that can be catalytically decomposed into hydrogen.

There are many types of FCs characterized by their electrolytes. One of the most promising ones to be utilized in electric vehicle applications is the polymer electrolyte membrane FC (PEMFC) because of its relatively small size, lightweight nature, and ease of construction [5,6]. In addition, PEMFC may also be used in residential and commercial power systems [7].

For the past 10 years, many works have been done on the utilizations of FCs in high power applications. Nowadays, the required FC power is in the range of 0.5-kW to 2-MW:

- 0.5-kW to 2-kW for unmanned aircrafts [8] and 40-kW to 700-kW for manned aircrafts [9,10];
- 50-kW to 100-kW for urban cars [11–14];
- 100-kW to 200-kW for buses and light tram [15–17];
- 600-kW to 1-MW for tramways and locomotives [18–20];
- 480-kW to 2-MW for distributed generation systems (grid parallel connection) [21–24].

The relatively short life of PEM fuel cells is a significant barrier to their commercialization in stationary and mobile applications. A longer life span for fuel cell components should be achieved to ensure high reliability, low maintenance costs and to justify fuel cells as economical alternative energy systems. Currently, the life-

* Corresponding author. Tel.: +66 2 913 2500x3332; fax: +66 2 587 8255.
E-mail addresses: Phatiphat.Thounthong@ensem.inpl-nancy.fr, phtt@kmutnb.ac.th (P. Thounthong).

0378-7753/$ – see front matter © 2008 Elsevier B.V. All rights reserved.
doi:10.1016/j.jpowsour.2008.12.120

time target requires PEM fuel cells to achieve 5000 h for mobile and 40,000 h for stationary applications [2].

The overall fuel cell performance decay rate, measured during continuous and uninterrupted operation, is the sum of both the stability and durability decay rates. Normal degradation targets require less than 10% loss in the efficiency of the fuel cell system at the end of life, and a degradation rate of 2–10 $\mu V\,h^{-1}$ is typically accepted for most applications [2].

According to Thounthong et al. [25,26] experimented on a 0.5-kW PEMFC (ZSW Company, Germany) and a 1.2-kW Nexa^{TM} PEMFC (Ballard Power System Company, Canada), Corrêa et al. [27] experimented on a 0.5-kW PEMFC (BCS Technology Company) and 0.5-kW PEMFC (Avista Company), Zhu et al. [28] experimented on a 0.5-kW PEMFC (Avista Company), Yoneyama et al. [29] experimented on a 100-kW PEMFC for railway vehicles, and Gaynor et al. [30] experimented on a 350-kW solid oxide FC, they point out the fact that the FC time constants are dominated by temperature and fuel delivery system (pumps, valves, and in some cases, a hydrogen reformer). As a result, fast energy demand will cause a high voltage drop in a short time, which is recognized as fuel starvation phenomenon [30,31]. Fuel or oxidant starvation refers to the operation of fuel cells at sub-stoichiometric reaction conditions. When starved from fuel or oxygen, the FC performance degrades and the cell voltage drops. This condition of operation is evidently hazardous for the FC stack [31,32].

Several factors can cause reactant starvation. A poor water management with flooding and a poor heat management during sub-zero temperatures and cold start-ups with ice within the cell can block the pores of the gas diffusion layers. A poor gas feeding management can lead to non-uniform distribution of the reactant gases resulting in partial or complete fuel and/or oxidant starvation or in sub-stoichiometric operation in individual cells, as already demonstrated in [32]. Reliability and lifetime are the most essential considerations in such power sources. Taniguchi et al. [32] clearly presented that hydrogen and oxygen starvation caused severe and permanent damage to the electro-catalyst of the fuel cell. They have recommended that fuel starvation must absolutely be avoided, even if the operation under fuel starvation is momentary, in just 1 s. In addition, an imperfect stack and cell design with an uneven distribution of mass in the flow fields, a poor stack assembly as well as quick load demands can be reasons contributing to gas starvation.

Thus, to utilize a FC in dynamic applications (such as in a cars, tramways or trains), its current or power slope must be limited to circumvent the fuel starvation problem, for example, $4\,A\,s^{-1}$ for a 0.5-kW, 12.5-V PEMFC [33]; a $2.5\,kW\,s^{-1}$ for a 40-kW, 70-V PEMFC [34]; and $5\,A\,s^{-1}$, $10\,A\,s^{-1}$ and $50\,A\,s^{-1}$ for a 20-kW, 48 V PEMFC [35]. Then, the electrical system must have at least an auxiliary power source (energy storage device), such as battery or supercapacitor, to improve the system performance when electrical loads at a dc bus demand high power in a short time (for example, vehicle acceleration and deceleration).

To illustrate vehicle characteristics, Fig. 1 depicts a speed and power profile of a European urban tramway (weight: 40–60 tons) during a drive cycle for a 500-m course. The acceleration and deceleration of the vehicle is sustained by electric motor drives with large power. One can observe the following:

- The vehicle positive peak power is around 600, and the negative peak power is around −800 kW.
- The positive and negative peak power durations are around 15 s and 10 s, respectively.
- The average power is between 100 kW and 200 kW according to the auxiliaries (heating or air conditioning).
- The duration of drive cycle is 67 s.

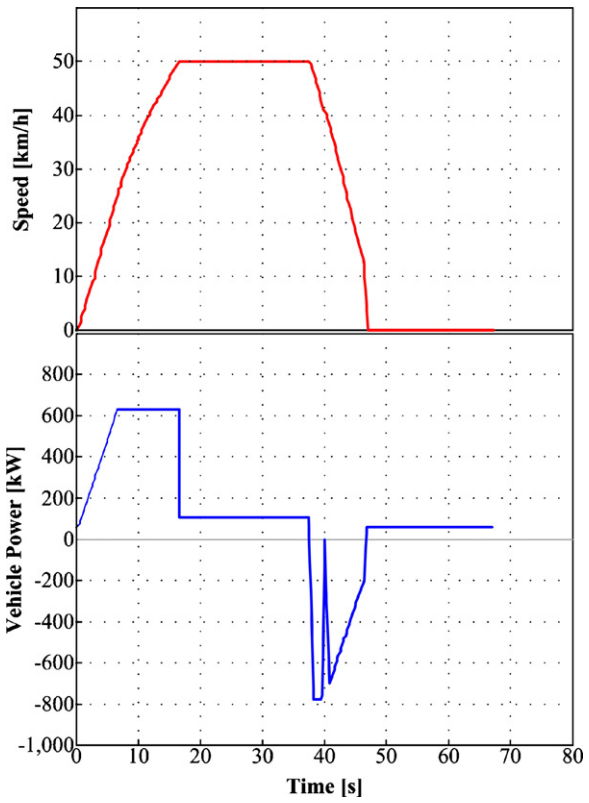

Fig. 1. Speed and power profile of a European urban tramway during a drive cycle for a 500-m course.

Thus, one can say that the drive cycle is with a high level of peak energy, a relative low average power, and duration around 67 s. Overall, the main power source operates most of the time at lower load. So, the hybridization consists in replacing the bulky generator of 600 kW, for example, with a smaller capable of providing the average power of 100 kW, and in coupling it with at least energy storage devices (typically batteries and supercapacitors) to provide the fluctuating power [36]. So, many recent works have already reported the structures of an FC/supercapacitor hybrid source [37,38] and an FC/battery hybrid source [39,40] for vehicle applications.

Energy storage technology is a main device in harvesting the kinetic energy that is wasted whenever vehicles or large machines must be slowed or stopped, called “regenerative braking energy”. Although batteries have been successfully used in light-duty vehicles, hybrid platforms for trucks, buses, tramways and trains will require storage and delivery of much higher powers than can be accommodated readily by batteries. Unlike batteries, new technology storage device of electrochemical capacitors (ECs) can operate at high charge and discharge rates over an almost unlimited number of cycles [1] and enable energy recovery in heavier duty systems.

Like all capacitors, ECs (also called supercapacitors “SuperC” or ultracapacitors because of their extraordinarily high capacitance density) physically store charge. Conventional electrostatic and electrolytic capacitors store charge on low-surface-area plates, but supercapacitors store charge in an electric double layer set up by ions at the interface between a high-surface area carbon electrode and a liquid electrolyte. Supercapacitors first appeared on the market in 1978 as farad-sized devices to provide computer memory backup power [1].

The very high capacitance of supercapacitors comes at a cost. The operating voltage of a supercapacitor cell cannot exceed the potential at which the electrolyte undergoes chemical reactions (typically

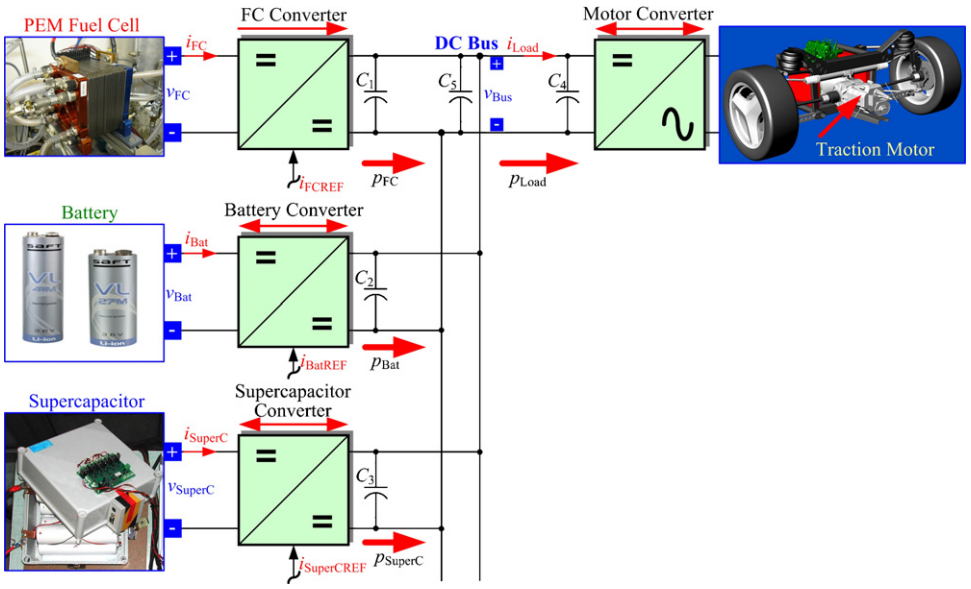

Fig. 2. Proposed structure of fuel cell/battery/supercapacitor hybrid power source. p_{FC} ($= v_{FC} \cdot i_{FC}$), v_{FC} and i_{FC} are the FC power, voltage, and current. P_{Bat} ($= v_{Bat} \cdot i_{Bat}$), v_{Bat} and i_{Bat} are the battery power, voltage, and current. P_{SuperC} ($= v_{SuperC} \cdot i_{SuperC}$), v_{SuperC} and i_{SuperC} are the supercapacitor power, voltage, and current. P_{Load} ($= v_{Bus} \cdot i_{Load}$), v_{Bus} and i_{Load} are the load power, dc bus voltage, and load current, respectively. i_{FCREF}, i_{BatREF}, and $i_{SuperCREF}$ are the current reference signals for FC, battery, and supercapacitor current control loops, respectively.

2.5–3 V per cell). For high voltage applications, supercapacitor cells, like batteries, can be series-connected.

One of the most important advantages of batteries over supercapacitors is their high energy density. They can store 3–30 times more charge. However, supercapacitors can deliver hundreds to many thousands of times the power of a similar-sized battery. Besides, the highly reversible electrostatic charge storage in supercapacitors does not produce the changes in volume that usually accompany the redox reactions of the active masses in batteries. Such volume changes are the main cause of the limited cycle life of batteries (around 1000 cycles for a lead-acid battery), compared to demonstrated full charge–discharge cycles for supercapacitors into the many millions.

Presented here is a perfect hybridization of the batteries and supercapacitors as energy storage devices with a PEM fuel cell as a main source. It deals with the conception and the achievement of a regulated dc bus voltage hybrid power. Its interest is focused on an energy management in system, presented in Section 2. To authenticate the proposed hybrid structure, a small-scale hardware system is realized by analog circuits and numerical calculation (dSPACE). Experimental results in Section 3 will illustrate the system performances.

2. Fuel cell/battery/supercapacitor hybrid power source

2.1. Structure of hybrid power source

A series hybrid electric vehicle is a vehicle supplied by several electrical sources. The power bus is a dc link between sources and load. FCs produce dc voltage outputs, and they are always connected to electric power networks through power conditioning units such as dc/dc and dc/ac converters. Power conversion and control functions form the basis of what has come to be known as the field of power electronics. In recent years, power electronics technology has been spurred by needs for efficient control of industrial applications and the development of more reliable lightweight switching power supplies for sophisticated system.

Different power converter topologies can be used for the power electronic interface between the fuel cell and the utility dc bus. For the dc link voltage level, it is depending on its applications:

- 270 V or 350 V for the standard on the all-electric aircraft [41];
- 48 V, 120 V, or 400 V to 480 V for stand-alone or parallel grid connections [42];
- 42 V (PowerNet) [5];
- 270–540 V for electric (fuel cell) vehicles [5,43];
- 350 V (transit bus systems) to 750 V (tramway and locomotive systems) [17–20].

There are many possible structures to connect a main source and two storage devices with the utility dc bus. The total mass, volume, cost and efficiency (optimization) of the propulsion system are investigated. One of the good solutions is depicted in Fig. 2. It is composed of a unidirectional converter (step-up converter) for a FC stack, bidirectional (2-quadrant) converters for battery and supercapacitor modules. It is the most sufficient configuration when comparing mass, volume and cost, as detailed in [44,45].

For reasons of safety and dynamics, these converters are primarily controlled by inner current regulation loops, classically [33,40]. These current control loops are supplied by three reference signals: $i_{SuperCREF}$, i_{BatREF}, and i_{FCREF}, generated by the energy management algorithm presented hereafter.

Note that the definitions of current direction are also illustrated in Fig. 2, and the dynamics of the current regulation loops are also supposed to be much faster than those of the outer voltage control loops, detailed hereafter. Thus, the currents i_{SuperC}, i_{Bat}, and i_{FCREF} are considered to follow perfectly their references $i_{SuperCREF}$, i_{BatREF}, and i_{FCREF}.

2.2. Energy management of hybrid power source

To manage the energy exchanges between the sources and the load at dc bus, three operating modes (or states) can be identified here again [33,40]:

(1) Charge mode, in which the main source supplies energy to the storage devices and to the load.
(2) Discharge mode, in which main source and storage devices supply energy to the load.
(3) Recovery mode, in which the load supplies energy to the storage devices.

As mentioned earlier, FC has slow dynamics. It can be compensated by faster dynamics from storage devices. Batteries have the best energy density but a bad power density. Contrary to batteries, supercapacitors have lower energy density (1000 times lower) but higher power density (100 times higher) and provide very fast dynamic cycles (close to 1 ms) [1,37].

Furthermore, battery lifetime depends on many factors: the operating temperature; the number and the depth of discharge cycles; rate and eventually the amount and number of rest in a discharged state and overcharge. To optimize the lifetime of the batteries, it is advisable to limit the battery current slope in order to ensure a longer battery lifetime. On the other hand, supercapacitors can provide more cycles than batteries (virtually infinite cycles) and are well suited to very fast dynamic cycles [46–50].

The energy management strategy based on a dynamic classification, as portrayed in Fig. 3, aims at distributing the global power mission of the vehicle (refer to Fig. 1) into the sources in such a way that each source is optimally used. According to the three points mentioned above embedded energy sources can be classified as illustrated in Fig. 3. Note that the power unit in Fig. 3 is the normalized unit (or per-unit [pu]). So, the defined dynamic classification depicted in Fig. 3 is obtained from our simulation result. FC generator is controlled as the lowest dynamic power source. The FC current or power slope must be limited to avoid the fuel starvation problem. Normally, the FC limited current or power slope has been experimentally determined as the highest slope of operated FC system, where no fuel starvation occurs, for example, 4 A s^{-1} for a 0.5-kW, 12.5-V PEMFC [33]; and a 2.5 kW s^{-1} for a 40-kW, 70-V PEMFC [34]. Supercapacitor is the highest dynamic power source, which provides the micro-cycles and the fast dynamic power supply. Battery is between FC and supercapacitor in the dynamic classification.

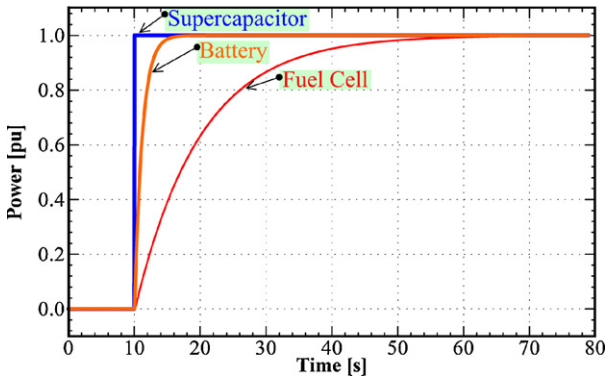

Fig. 3. Dynamic classification of the embedded sources.

Thounthong et al. [33,37] who studied a FC/supercapacitor hybrid source have proposed the hybrid energy management by regulating a dc bus voltage. Therefore, the proposed hybrid energy management here is shown in Fig. 4. Its basic principle here lies in using the supercapacitors (the fastest energy source), for supplying energy required to achieve the dc link voltage regulation. The batteries are controlled as the power source (with dynamic limitations, F_2) that supplies energy to the supercapacitors to keep them charged. Then, the FC, although obviously the main energy source of the system, is functioned as the generator (with dynamic limitations, F_1) that supplies energy to the batteries to keep them charged.

Consequently, the supercapacitor converter is driven to realize a classical dc bus voltage regulation. The battery converter is driven to maintain the supercapacitors at a given state-of-charge, here the

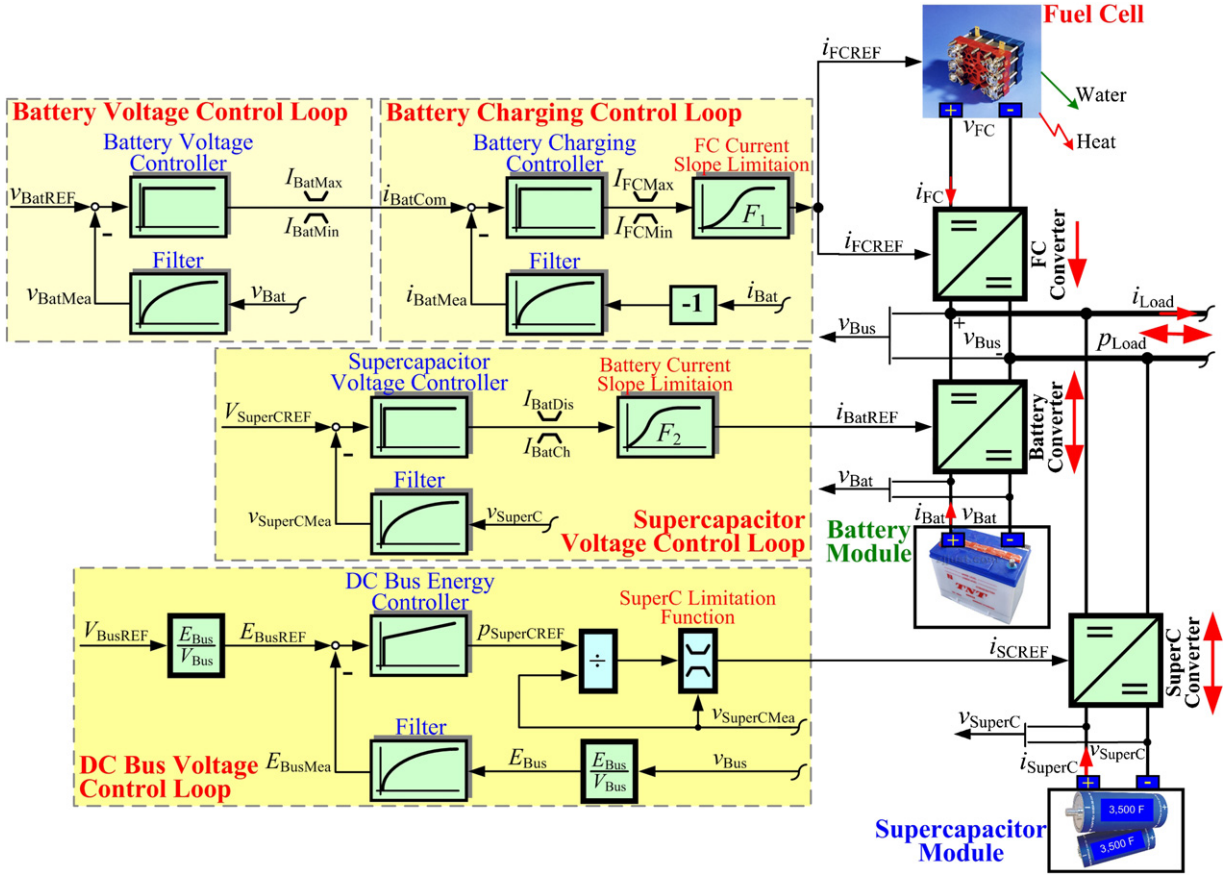

Fig. 4. Proposed energy management of the fuel cell/battery/supercapacitor hybrid power source.

supercapacitor voltage regulation. Then, the FC converter is also driven to maintain the batteries at a given state-of-charge, here the battery voltage regulation. As a result, the hybrid system composes of three-controlled variables:

- the dc bus voltage v_{Bus},
- the supercapacitor voltage v_{SuperC}, and
- the battery voltage v_{Bat}.

and three-control variables:

- the supercapacitor current reference $i_{SuperCREF}$,
- the battery current reference i_{BatREF}, and
- the FC current reference i_{FCREF}.

As depicted in Fig. 2, one may write the classical power conservative law (without losses) of the FC/battery/supercapacitor hybrid power source as follow:

$$p_{Load}(t) = p_{SuperC}(t) + p_{Bat}(t) + p_{FC}(t) \quad (1)$$

where p_{Load} is the load power, p_{SuperC} is the supercapacitor power, p_{Bat} is the battery power, and p_{FC} is the fuel cell power.

2.2.1. DC bus voltage control loop

The dc bus voltage control loop considers a dc bus capacitive energy E_{Bus} as state variable, and the supercapacitor delivered power as command variable, to obtain a natural linear transfer function for the system [37]. If the losses in the FC, battery, and supercapacitor converters are neglected, the dc link capacitive energy is given versus supercapacitor power p_{SuperC}, battery power p_{Bat}, FC power p_{FC} and load power p_{Load} by the following differential equation:

$$\frac{dE_{Bus}(t)}{dt} = p_{SuperC}(t) + p_{Bat}(t) + p_{FC}(t) - p_{Load}(t) \quad (2)$$

which shows that the transfer function "E_{Bus}/p_{SC}" is a pure integrator [37]. The dc bus energy measurement is carried out by means of the following classical calculation:

$$E_{Bus}(t) = \frac{1}{2} \cdot C_{Bus} \cdot v_{Bus}^2(t) \quad (3)$$

where C_{Bus} is the total capacitance of capacitors at the dc bus (refer to Fig. 2, $C_{Bus} = C_1 + C_2 + C_3 + C_4 + C_5$). It enables the generation of both bus energy reference and bus energy measurement, through dc bus voltage reference v_{BusREF} and dc bus voltage v_{Bus}, respectively. Supercapacitor power reference $p_{SuperCREF}$ is generated by means of a proportional–integral (PI)-controller. So, a first-order filter is used for E_{Bus} to reduce harmonics due to switching. $p_{SuperCREF}$ is then divided by the measured supercapacitor voltage $v_{SuperCMea}$, and limited to maintain supercapacitor voltage within an interval $[V_{SuperCMin}, V_{SuperCMax}]$. The upper value $V_{SuperCMax}$ of this interval corresponds to the maximum voltage of the storage device, and the lower value $V_{SuperCMin}$, traditionally equal to $V_{SuperCMax}/2$, to a level under which supercapacitor discharge becomes ineffective. This results in the supercapacitor current reference i_{SCREF}.

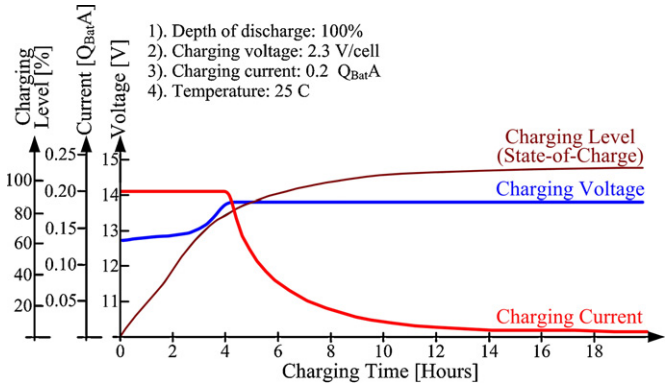

Fig. 5. Constant current–constant voltage charging of a lead-acid battery.

The supercapacitor current–voltage saturation function called "SuperC Limitation Function" as portrayed in Fig. 4, consists of limiting the reference $i_{SuperCREF}$ to the interval [maximum charging current $I_{SuperCMin}$ (negative value), maximum discharging current $I_{SuperCMax}$ (positive value)] defined, versus the measured supercapacitor voltage $v_{SuperCMea}$ as follows [33]:

$$\begin{cases} I_{SuperCMin} = -I_{SuperCRated} \cdot \min\left(1, \dfrac{V_{SuperCMax} - V_{SuperCMea}}{\Delta v}\right) \\ I_{SuperCMax} = +I_{SuperCRated} \cdot \min\left(1, \dfrac{V_{SuperCMea} - V_{SuperCMin}}{\Delta v}\right) \end{cases} \quad (4)$$

where, $I_{SuperCRated}$ and Δv are the regulation parameters.

2.2.2. Supercapacitor voltage control loop

As presented in Fig. 4, a proportional (P)-controller is sufficient for the supercapacitor voltage control loop, as far as the proportional gain is high enough to introduce only a little static error. So, a first-order filter is used for supercapacitor voltage measurement, to reduce switching harmonics. The output signal from the regulator must be limited in level and slope, to respect constraints associated with the battery. Then the battery reference signal i_{BatREF} that drives the battery converter through the battery current control loop is then kept within an interval [maximum discharging current I_{BatDis} (positive value), maximum charging current I_{BatCh} (negative value)]. Moreover, the "Battery Current Slope Limitation" at a delay F_2 enables safe operation of the battery, even during transient power demand. To obtain a natural linear transfer function, a second-order delay (filter) F_2 is chosen for the battery current dynamics as follow:

$$F_2(s) = \frac{1}{(s/\omega_{n2})^2 + (2 \cdot \zeta_2/\omega_{n2})s + 1} \quad (5)$$

where ω_{n2} and ζ_2 are the regulation parameters. So, a delay F_2 of the battery dynamics must be faster than a delay F_1 of the FC dynamics, refer to Figs. 3 and 4.

2.2.3. Battery voltage control loop

The proposed battery voltage control loop is also portrayed in Fig. 4. The simple method to charge the battery is the constant current–constant voltage (CCCV) charging as depicted in Fig. 5 [40], where Q_{Bat} is the battery capacity. The battery current is constant (maximum battery charging current I_{BatMax} is set around $Q_{Bat}/5$–$Q_{Bat}/10$; for a Li-ion battery, it can be set at $I_{BatMax} = Q_{Bat}$) when the actual battery voltage v_{Bat} is far from the battery voltage reference v_{BatREF} and reduced current when v_{Bat} is near v_{BatREF} and zero when v_{Bat} is equal to v_{BatREF} (Fig. 5). Note here that a similar structure of the battery charging algorithm based on battery state-of-charge *SOC* has been reported in [40]. So, the main problem is that the battery capacity Q_{Bat} is not constant. It is dependent on many factors as follows [40]:

- the depth of discharge,
- discharge rate,
- cell temperature,
- charging regime,
- dwell time at low and high *SOC*,
- battery maintenance procedures,
- current ripple, and
- amount and frequency of overcharge.

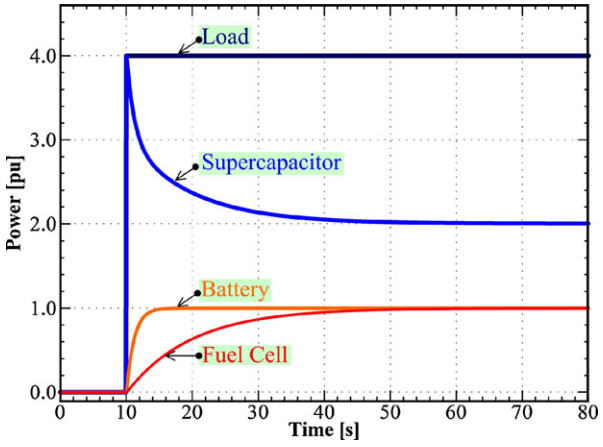

Fig. 6. Simulation result: hybrid source response during a high positive load step.

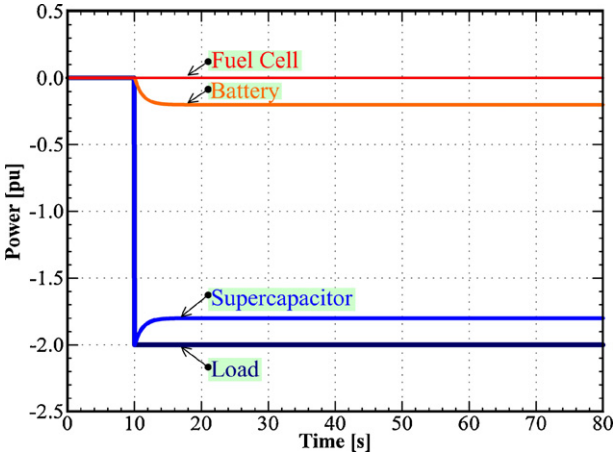

Fig. 7. Simulation result: Hybrid source response during a high negative load step (imitated regenerative braking).

As a result, the battery voltage is here considered as a battery *SOC*. According to the proposed battery charging algorithm here, a P-controller is enough to generate a battery charging current. This signal must be limited within an interval [maximum charging current I_{BatMax} (equal to $-1{\cdot}I_{BatCh}$), maximum discharging current I_{BatMin} (equal to $-1{\cdot}I_{BatDis}$). The measured battery current must be inversed because the definition of battery current is negative for charging current.

2.2.4. Battery charging control loop

The battery charging control loop receives i_{BatCOM} from a battery voltage regulation loop as illustrated in Fig. 4. A P-controller is sufficient to generate the FC current reference i_{FCREF}. It must be limited in level, within an interval [maximum FC current I_{FCMax} (corresponding to a FC rated current), minimum FC current I_{FCMin} (set to 0 A)] and limited in slope, which enables the safe operation of the FC in order to respect constraints associated with the FC, as far as the proportional gain is high enough to introduce only a small static error.

A first-order low-pass filter is used for the battery current measurement to reduce ripple current coming from the switching frequency. Moreover, the "FC Current Slope Limitation" at a delay F_1 enables safe operation of the FC. To obtain a linear transfer function, a second-order delay (filter) F_1 is also chosen for the FC current dynamics as:

$$F_1(s) = \frac{1}{(s/\omega_{n1})^2 + (2 \cdot \zeta_1/\omega_{n1})s + 1} \quad (6)$$

where ω_{n1} and ζ_1 are the regulation parameters.

2.2.5. Conclusion of proposed control algorithm

Using this form of control, the state of the supercapacitors is naturally defined, through the dc link voltage regulation, by the load power level and by its state-of-charge. In narrow steady-state conditions:

(1) if load power is negative, the dc link voltage regulation generates a negative $i_{SuperCREF}$;
(2) if load power is positive greater than the approximate FC rated power summing with the battery rated power, the dc link voltage regulation generates a positive i_{SCREF};
(3) otherwise, the state of the supercapitors depends on its state-of-charge: supercapacitor current will therefore be positive if $v_{SuperC} > V_{superCREF}$, negative if $v_{SuperC} < V_{SuperCREF}$.

In all cases, battery state depends on supercapacitor voltage and its voltage. FC state depends only on battery voltage. The FC current will be strictly positive and less than $I_{FCRated}$. Otherwise it will be zero.

In transient conditions, as FC and battery power dynamics have been intentionally reduced by F_1 and F_2, the supercapacitor supplies load variations. In effect, the dc bus voltage regulation transforms a sudden increase in load power into a sudden increase of supercapacitor current, and on the contrary a sudden decrease in load power into a sudden decrease of supercapacitor current.

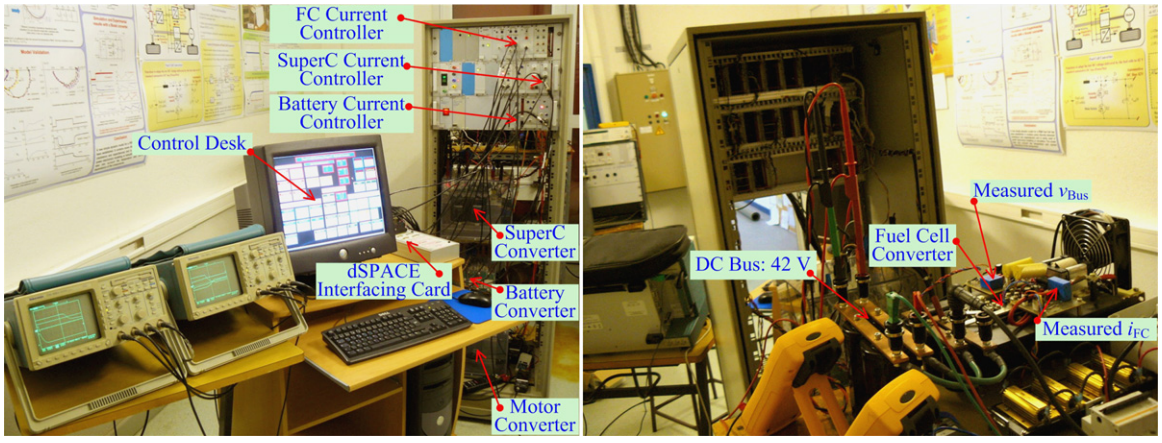

Fig. 8. Test bench of the fuel cell/battery/supercapacitor hybrid power source.

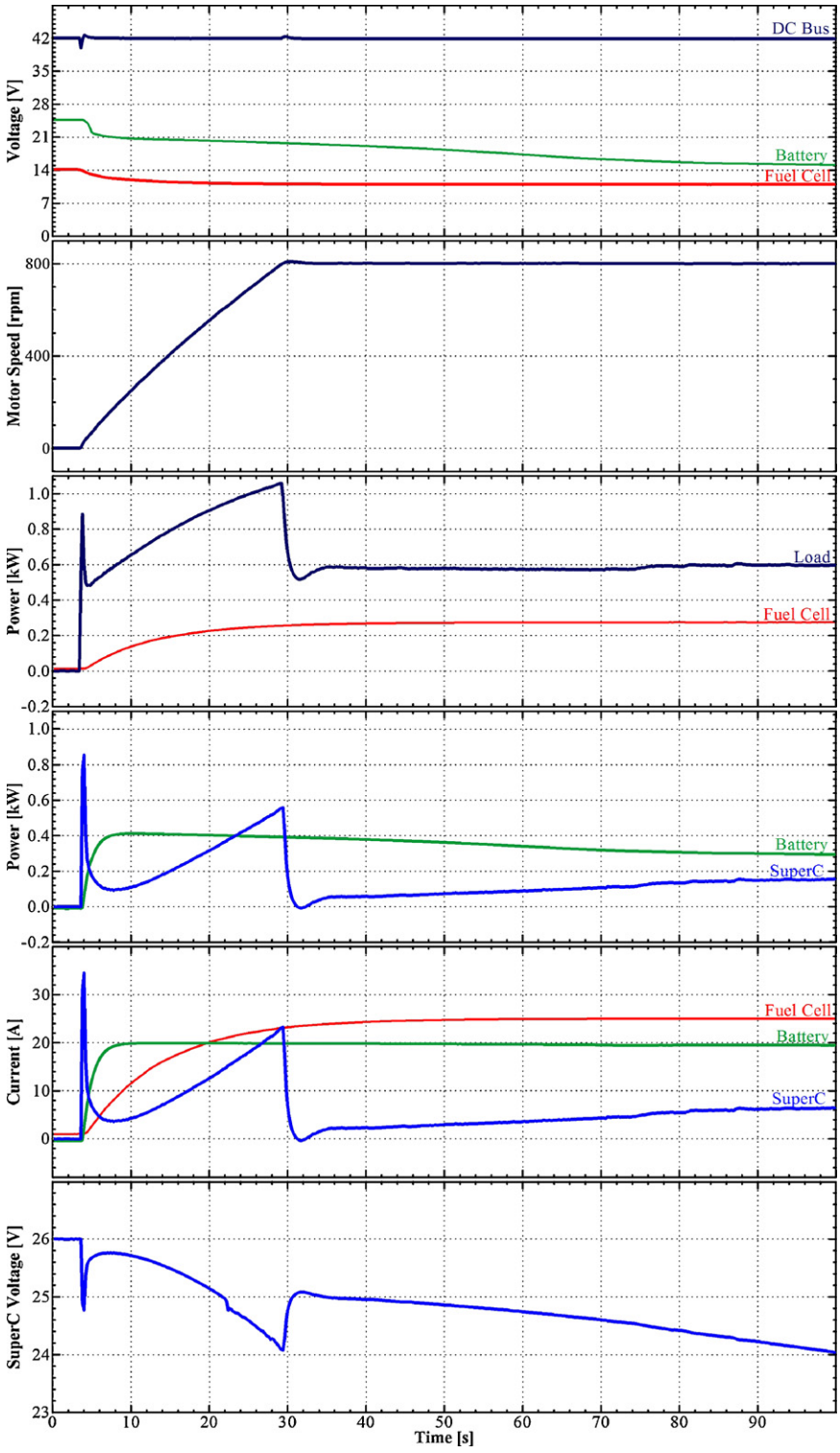

Fig. 9. Hybrid source response during motor starting to a final speed of 800 rpm.

Finally, Figs. 6 and 7 present simulation results during a high constant stepped load power. There are the load, supercapacitor, battery, and fuel cell power. In simulation, the FC minimum and maximum powers are set at 0.0 pu and 1.0 pu, respectively, and the battery minimum and maximum powers are set at −0.2 pu (corresponding to the maximum charging current) and 1.0 pu (corresponding to the maximum discharging current), respectively. As illustrated in Fig. 6, initially the supercapacitor and battery modules are full-of-charge, the load power is zero. As a result, the fuel cell, battery, and supercapacitor powers are zero. At $t = 10$ s, the constant load power steps to 4.0 pu. One can observe the following:

- The supercapacitor module supplies most of the transient power required.
- The supercapacitor power is the fastest dynamics; the battery power is in the middle dynamics; then the FC power is the slowest dynamics.

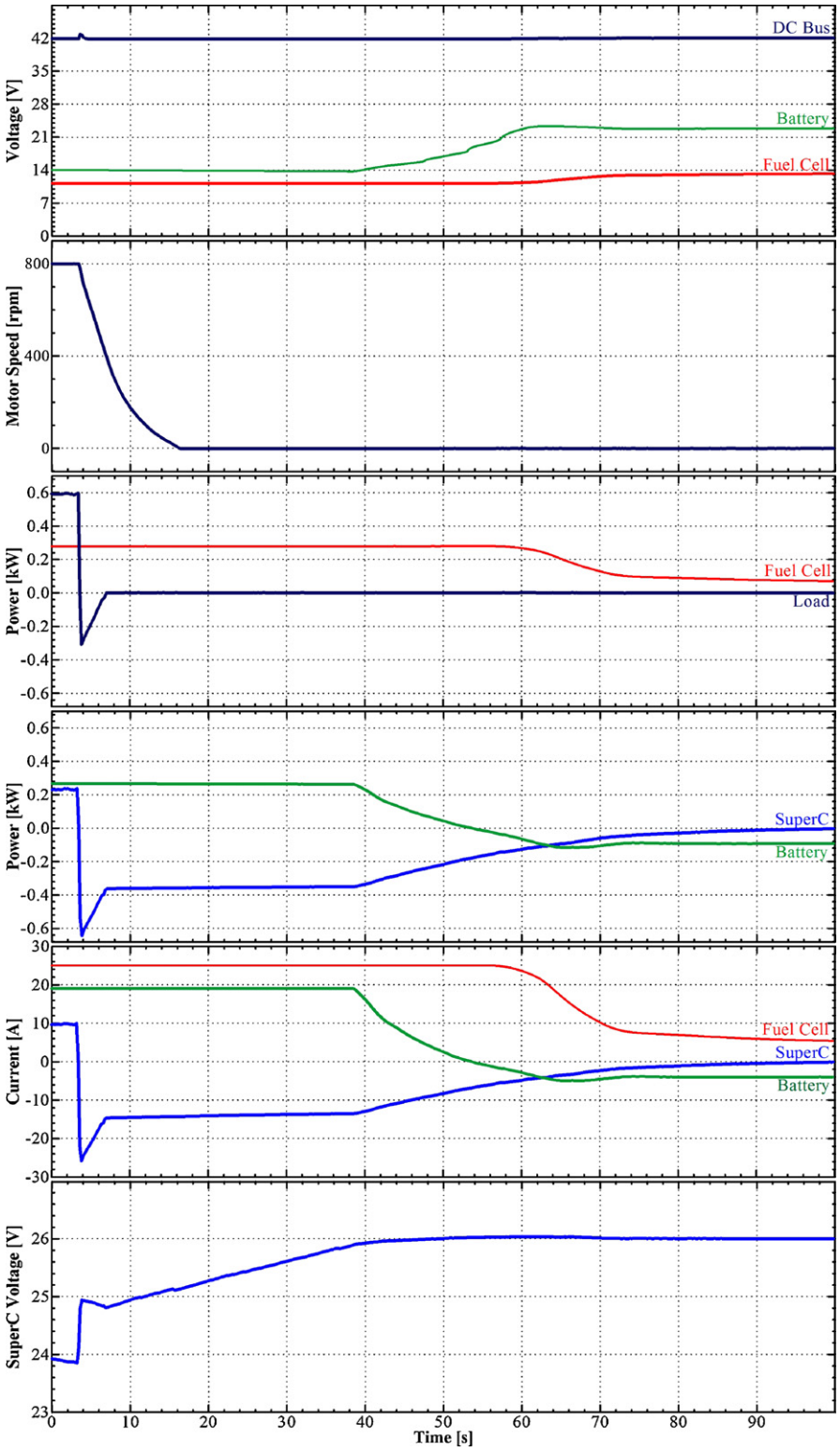

Fig. 10. Hybrid source response during motor braking from an initial speed of 800 rpm to stop.

- Synchronously, the supercapacitor power, after a sharp increase (discharging), decreases slowly to a constant discharge at 2.0 pu.
- At steady-state, the constant load power of 4.0 pu is entirely supplied by the FC of 1.0 pu, the battery of 1.0 pu (discharging state), and the supercapacitor of 2.0 pu (discharging state).

As a final simulation illustrated in Fig. 7, initially the supercapacitor and battery modules are full-of-charge, the load power is zero. As a result, the fuel cell, battery, and supercapacitor powers are zero. At $t = 10$ s, the constant load power steps to -2.0 pu (imitated regenerative braking). One can see again the following:

- The supercapacitor module supplies most of the transient power required.
- The supercapacitor power is the fastest dynamics, and then following by the battery power.

- The FC power is still zero power, because the FC power source is a unidirectional power flow.
- Simultaneously, the supercapacitor power, after a sharp decrease (charging), increases slowly to a constant charge at −1.8 pu.
- At steady-state, the constant regenerative braking power of −2.0 pu is entirely absorbed by the battery of −0.2 pu (charging state), and the supercapacitor power of −1.8 pu (charging state).

3. Experimental validation

3.1. Test bench description

A PEM fuel cell system (500 W, 50 A) studied here was constructed by the Zentrum für Sonnenenergie und Wasserstoff-Forschung (ZSW) Company, Germany. It is composed of 16 cells in series with area of 100 cm^2. It is supplied with pure hydrogen from bottles under pressure and with clean, dry air from a compressor. Storage devices are obtained by means of two lead-acid batteries (68 Ah, 12 V) connected in series, and twelve supercapacitors (3500 F, 2.5 V, 500 A) developed and manufactured by the SAFT Company, France connected in series. In addition, a small-scale test bench in our laboratory is presented in Fig. 8.

The FC converter is a classical boost converter [25]. The battery and supercapacitor converters are bidirectional (2-quadrant) converters [33]. The load at dc link is only a traction motor drive of 2 kW coupled with a small-inertia flywheel.

The dc bus studied here is 42 V (PowerNet) [5]. For the supercapacitor, battery, and FC current control loops, they have been realized by analog circuits to function at high bandwidth. For the dc bus voltage, the supercapacitor voltage, the battery voltage, and the battery charging regulation loops have been implemented in the real time card dSPACE DS1104, through the mathematical environment of Matlab–Simulink, with a sampling frequency of 25 kHz. The ControlDesk™ software enables changes in the parameters of the control loops. The measurements of the dc bus voltage v_{Bus}, the supercapacitor voltage v_{SuperC}, supercapacitor current i_{SuperC}, the battery voltage v_{Bat}, the battery current i_{Bat}, and the FC current i_{FC} have been realized by means of zero-flux Hall effect sensors.

The voltage reference signals are set as follows:

- V_{BusREF} = 42 V,
- V_{BatREF} = 25 V,
- $V_{SuperCREF}$ = 26 V.

For the minimum and maximum controlled parameters are set as follows:

- $I_{SuperCRated}$ = 200 A,
- $V_{SuperCMin}$ = 15 V,
- $V_{SuperCMax}$ = 30 V,
- $\Delta v = 0.5$ V,
- I_{BatCh} = −6 A,
- I_{BatDis} = +20 A,
- I_{BatMax} = 6 A,
- I_{BatMin} = −20 A,
- I_{FCMin} = 0 A,
- I_{FCMax} = 25 A.

Note here that for safety reasons the maximum FC current I_{FCMax} is set at 25 A (around 280 W) in place of 50 A (rated current).

3.2. Experimental results

Figs. 9 and 10 portray waveforms obtained during a motor drive cycle. They present the dc bus, supercapacitor, battery, and FC voltages; supercapacitor, battery, and FC currents; load (or approximately as a motor power), supercapacitor, battery, and FC powers; and motor speed.

As portrayed in Fig. 9. the initial state is zero for the load, supercapacitor, battery, and fuel cell powers. It means that the supercapacitor and battery modules are full of charge. One can observe the supercapacitor voltage is equal to the supercapacitor voltage reference of 26 V, and battery voltage is equal to the battery voltage reference of 25 V. At t = 4 s, the motor starts to the final speed of 800 rpm, so that the steady-state load power supplies by the FC, battery, and supercapacitor sources. It can be observed the following:

- The supercapacitor module supplies most of the transient power required during motor acceleration.
- The supercapacitor power is the fastest dynamics; the battery power is in the middle dynamics; then the FC power is the slowest dynamics.
- Synchronously, the supercapacitor power, after a sharp increase (discharging) during motor acceleration, decreases slowly to a constant discharge at around 160 W.
- The steady-state load power is approximately 600 W, totally supplied by the FC, battery, and supercapacitor sources. The FC operates at a maximum current of 25 A, and the battery module is in the state of discharge with the constant discharging current I_{BatDis} of 20 A.

As a final test, Fig. 10 presents waveforms obtained at motor braking from an initial speed of 800 rpm to stop at t = 4 s. One can scrutinize the regenerative braking energy from the traction motor supplies back to the dc bus, demonstrating four phases as follows:

- First, the supercapacitor recovers the energy supplied to the dc link by the FC, the battery, and the motor regenerative braking.
- Second, the FC supplies power for charging the supercapacitor and battery storage devices.
- Third, when the supercapacitor module is nearly full of charge, the FC power slowly reduces to charging only the battery module.
- Fourth, the supercapacitor module is full of charge ($V_{SuperCREF} = v_{SuperC}$). Consequently, the FC supplies energy for only charging the battery.

Excellently, only little perturbations on the dc bus voltage can be seen during motor start/stop and the dynamics of FC and battery powers are reduced, which is of major importance in the proposed energy management hybrid power source.

4. Conclusions

The key objective of this present work is to propose an original control algorithm for a dc distributed generation supplied by a fuel cell main source, and the perfect storage devices: supercapacitors and batteries. The combined utilization of batteries and supercapacitors is the perfect hybridization system of a high energy and high power density. The study mainly focuses on the FC, battery and supercapacitor taking account of the intrinsic energetic characteristics of these sources (i.e. energy and power densities, typical operating dynamics) in the energy management strategy. Hence, the control principle presents how to stay away from the fast transition of the FC and battery powers, and then reducing the FC and battery stresses. As a result, hybrid power source will increase its lifetime.

Experimental results in our laboratory carried out using a small-scale test bench, which employs a PEMFC (500 W, 50 A), and storage devices composed of supercapacitor bank (292 F, 30 V) and

lead-acid battery module (68 Ah, 24 V), corroborate the excellent performances of the proposed energy management during a motor drive cycle. During motor starts/stops or other significant steps in load, the storage elements provide the balance of energy needed during the momentary load transition period; and also absorbs excess energy from regenerative braking.

Acknowledgments

The authors gratefully acknowledge the French National Center for Scientific Research (CNRS), the Groupe de Recherche en Electrotechnique et Electronique de Nancy (GREEN: UMR 7037), the Thailand Research Fund (TRF Grant number: MRG5180348), and the Thai-French Innovation Institute (TFII) for supporting this project. The research work is in cooperative research program under the "Franco-Thai on higher education and research joint project". The authors also would like to thank Prof. M. Hinaje for operating the FC system during experimentations in the GREEN laboratory.

References

[1] P. Thounthong, B. Davat, S. Raël, IEEE Power Energy 6 (2008) 69–76.
[2] W. Schmittinger, A. Vahidi, J. Power Sources 180 (2008) 1–14.
[3] W.K. Na, B. Gou, IEEE Trans. Energy Convers. 23 (2008) 179–190.
[4] M. Romer, G.H. Miley, N. Luo, R.J. Gimlin, IEEE Trans. Energy Convers. 23 (2008) 171–178.
[5] A. Emadi, Y.J. Lee, K. Rajashekara, IEEE Trans. Ind. Electron. 55 (2008) 2237–2245.
[6] K.P. Adzakpa, K. Agbossou, Y. Dubé, M. Dostie, M. Fournier, A. Poulin, IEEE Trans. Energy Convers. 23 (2008) 581–591.
[7] M.C. Péra, D. Candusso, D. Hissel, J.M. Kauffmann, IEEE Ind. Electron. Mag. 1 (2007) 28–37.
[8] T.H. Bradley, B.A. Moffitt, D.N. Mavris, D.E. Parekh, J. Power Sources 171 (2007) 793–801.
[9] N.L. Rey, J. Mosquera, E. Bataller, F. Ort, C. Dudfield, A. Orsillo, J. Power Sources 181 (2008) 353–362.
[10] K. Rajashekara, J. Grieve, D. Daggett, IEEE Ind. Appl. Mag. 14 (2008) 54–60.
[11] R. von Helmolt, U. Eberle, J. Power Sources 165 (2007) 833–843.
[12] T. Aicher, B. Lenz, F. Gschnell, U. Groos, F. Federici, L. Caprile, L. Parodi, J. Power Sources 154 (2006) 503–508.
[13] R.M. Moore, K.H. Hauer, S. Ramaswamy, J.M. Cunningham, J. Power Sources 159 (2006) 1214–1230.
[14] P. Fontela, A. Soria, J. Mielgo, J.F. Sierra, J. de Blas, L. Gauchia, J.M. Martinez, J. Power Sources 169 (2007) 184–193.
[15] S. Varigonda, M. Kamat, Comput. Chem. Eng. 30 (2006) 1735–1748.
[16] M. Saxe, A. Folkesson, P. Alvfors, Energy 33 (2008) 689–711.
[17] M. Kim, Y.J. Sohn, W.Y. Lee, C.S. Kim, J. Power Sources 178 (2008) 706–710.
[18] A.R. Miller, K.S. Hess, D.L. Barnes, T.L. Erickson, J. Power Sources 173 (2007) 935–942.
[19] A.R. Miller, J. Peters, B.E. Smith, O.A. Velev, J. Power Sources 157 (2006) 855–861.
[20] T. Ogawa, H. Yoshihara, S. Wakao, K. Kondo, M. Kondo, Proceeding of the EPE 2007 – 12th European Conference on Power Electronics and Applications, Aalborg, Denmark, 2–5 September 2007, pp. 1–8.
[21] K.N. Reddy, V. Agarwal, IEEE Trans. Energy Convers. 22 (2007) 666–673.
[22] M. Tekin, D. Hissel, M.C. Péra, J.M. Kauffmann, IEEE Trans. Ind. Electron. 54 (2007) 595–603.
[23] J.W. Jung, A. Keyhani, IEEE Trans. Energy Convers. 22 (2007) 467–476.
[24] C. Wang, M.H. Nehrir, IEEE Trans. Energy Convers. 22 (2007) 864–872.
[25] P. Thounthong, S. Raël, B. Davat, J. Power Sources 153 (2006) 145–150.
[26] P. Thounthong, P. Sethakul, S. Raël, B Davat, Proceedings of the 39th IEEE Power Electronics Specialists Conference (PESC), Island of Rhodes, Greece, 15–19 June, 2008, pp. 230–236.
[27] J.M. Corrêa, F.A. Farret, V.A. Popov, M.G. Simões, IEEE Trans. Energy Convers. 20 (2005) 211–218.
[28] T. Zhu, S.R. Shaw, S.B. Leeb, IEEE Trans. Energy Convers. 21 (2006) 195–201.
[29] T. Yoneyama, T. Yamamoto, K. Kondo, T. Furuya, K. Ogawa, Proceeding of the EPE 2007 – 12th European Conference on Power Electronics and Applications, Aalborg, Denmark, 2–5 September 2007, pp. 1–10.
[30] R. Gaynor, F. Mueller, F. Jabbari, J. Brouwer, J. Power Sources 180 (2008) 330–342.
[31] J. Wu, X.Z. Yuan, J.J. Martin, H. Wang, J. Zhang, J. Shena, S. Wu, W. Merida, J. Power Sources 184 (2008) 104–119.
[32] A. Taniguchi, T. Akita, K. Yasuda, Y. Miyazaki, J. Power Sources 130 (2004) 42–49.
[33] P. Thounthong, S. Raël, B. Davat, J. Power Sources 158 (2006) 806–814.
[34] P. Rodatz, G. Paganelli, A. Sciarretta, L. Guzzella, Control Eng. Pract. 13 (2005) 41–53.
[35] P. Corbo, F. Migliardini, O. Veneri, J. Power Sources 181 (2008) 363–370.
[36] C. Wang, M.H. Nehrir, IEEE Trans. Energy Convers. 23 (2008) 957–967.
[37] P. Thounthong, S. Raël, B. Davat, IEEE Trans. Ind. Electron. 54 (2007) 3225–3233.
[38] M. Uzunoglu, M.S. Alam, IEEE Trans. Energy Convers. 23 (2008) 263–272.
[39] Z. Jiang, L. Gao, R.A. Dougal, IEEE Trans. Energy Convers. 22 (2007) 507–515.
[40] P. Thounthong, S. Raël, B. Davat, IEEE Trans. Energy Convers. 23 (2008) 148–155.
[41] J. Dollmayer, N. Bundschuh, U.B. Carl, Aerospace Sci. Technol. 10 (2006) 686–694.
[42] S.Y. Choe, J.W. Ahn, J.G. Lee, S.H. Baek, IEEE Trans. Energy Convers. 23 (2008) 669–680.
[43] S.M. Lukic, J. Cao, R.C. Bansal, F. Rodriguez, A. Emadi, IEEE Trans. Ind. Electron. 55 (2008) 2258–2267.
[44] E. Schaltz, S.J. Andreasen, P.O. Rasmussen, Proceeding of the EPE 2007 – 12th European Conference on Power Electronics and Applications, Aalborg, Denmark, 2–5 September 2007, pp. 1 – 10.
[45] A. Stepanov, I. Galkin, L. Bisenieks, Proceeding of the EPE 2007 – 12th European Conference on Power Electronics and Applications, Aalborg, Denmark, 2–5 September 2007, pp. 1–7.
[46] A. Kusko, J. Dedad, IEEE Ind. Appl. Mag. 13 (2007) 66–72.
[47] S.K. Mazumder, S.K. Pradhan, J. Hartvigsen, IEEE Trans. Energy Convers. 22 (2007) 457–466.
[48] H. Tao, J.L. Duarte, M.A.M. Hendrix, IEEE Trans. Ind. Electron. 55 (2008) 3012–3021.
[49] J. Bauman, M. Kazerani, IEEE Trans. Veh. Technol. 57 (2008) 760–769.
[50] T. Montanié, Proceeding of the EPE 2003 – 10th European Conference on Power Electronics and Applications, Toulouse, France, 2–4 September 2003, pp. 1–10.